Smart Grid and Renewable Energy, 2024, 15, 217-247
https://www.scirp.org/journal/sgre
ISSN Online: 2151-4844
ISSN Print: 2151-481X

Performance of a Combined Energy System Consisting of Solar Collector, Biogas Dry Reforming and Solid Oxide Fuel Cell: An Indian Case Study

Akira Nishimura[1], Ryotaro Sato[1], Ryota Nakajima[1], Eric Hu[2]

[1]Division of Mechanical Engineering, Graduate School of Engineering, Mie University, Tsu, Japan
[2]School of Electrical Mechanical Engineering, the University of Adelaide, Adelaide, Australia
Email: nisimura@mach.mie-u.ac.jp

How to cite this paper: Nishimura, A., Sato, R., Nakajima, R. and Hu, E. (2024) Performance of a Combined Energy System Consisting of Solar Collector, Biogas Dry Reforming and Solid Oxide Fuel Cell: An Indian Case Study. *Smart Grid and Renewable Energy*, **15**, 217-247.
https://doi.org/10.4236/sgre.2024.1510013

Received: August 30, 2024
Accepted: October 21, 2024
Published: October 24, 2024

Abstract

An energy production system consisting of a solar collector, biogas dry reforming reactor and solid oxide fuel cell (SOFC) was assumed to be installed in Kolkata, India. This study aims to understand the impact of climate conditions on the performance of solar collectors with different lengths of parabolic trough solar collector (dx) and mass flow rate of heat transfer fluid (m). In addition, this study has evaluated the amount of H_2 produced by biogas dry reforming (G_{H2}), the amount of power generated by SOFC (P_{SOFC}) and the maximum number of possible households (N) whose electricity demand could be met by the energy system proposed, considering the performance of solar collector with the different dx and m. As a result, the optimum dx was found to be 4 m. This study revealed that the temperature of heat transfer fluid (T_{fb}) decreased with the increase in m. T_{fb} in March, April and May was higher than that in other months, while T_{fb} from June to December was the lowest. G_{H2}, P_{SOFC} and N in March, April and May were higher than those in other months, irrespective of m. The optimum m was 0.030 kg/s.

Keywords

Solar Collector, Temperature of Simulated Biogas, Case Study of Installation in India, H_2 Production by Dry Reforming, Power Generated by SOFC

1. Introduction

Energy consumption has been increasing rapidly with the rapid economic development. According to the Energy White Paper [1], the energy consumption was

14.4 billion ton based on equivalent of oil in 2022. On the other hand, renewable energy is being paid attention to in order to introduce a mode to meet the increase in energy consumption as well as to solve the global warming problem. According to the data base [1], the ratio of renewable energy including hydro to total energy consumption was 14.2% in 2022 [1]. It is expected that renewable energy will increase worldwide.

Using renewable energy to produce H_2 is a promising way to utilize renewable energy. There are several approaches to produce H_2, including producing H_2 from biogas dry reforming. Biogas, which consists of CH_4 (ratio: 55 - 75 vol%) and CO_2 (ratio: 25 - 45 vol%) [2] can be produced by fermentation of the action of anaerobic microorganisms on raw materials such as garbage, livestock and sewage sludge. It is known from the International Energy Agency [3] that the biogas equivalent to 1.46 EJ was produced in 2020. According to the International Energy Agency [3], the amount of produced biogas based on energy value was approximately five times as large as that in 2000. We can expect that the produced biogas will increase more and more. Biogas is usually used as a fuel for gas engine and micro gas turbine [4]. However, the power generation is smaller than using a natural gas due to consisting of CO_2 of approximately 40 vol%. In this study, a biogas is proposed to be used as a feedstock to produce H_2 via a thermally powered biogas dry reforming process. The produced H_2 can be used as a fuel for solid oxide fuel cell (SOFC) [5]. CO, which is a by-product of biogas dry reforming can also be used as a fuel for SOFC, resulting a more effective energy production system.

This study proposes a system combining the above described energy production system with a solar collector to supply the heat, which is needed for a biogas dry reforming, because it is an endothermic reaction. There are some studies reporting the combined system with a solar collector to produce H_2 using a heat for the chemical reaction [6]-[14]. The numerical investigation of the effect of peak heat flux, inlet flow rate and CH_4/CO_2 feed ratio on reaction temperature, reaction rates, conversion of syngas, syngas yield, carbon deposition, and other thermochemical characteristics of the porous material filled in solar collector under high-flux concentrated irradiation was reported [6]. The peak heat flux over 0.734 MW/m^2 would decrease CH_4 conversion and H_2 yield, resulting in the reduction of the syngas yield. The experimental study using solar scheffler collector for biogas dry reforming was conducted [7]. The parabolic solar collector which could increase the temperature of biogas from 383 K to 773 K performed H_2 yield of 16% and CO yield of 10%. The solar thermochemical system including a parabolic trough solar collector and a membrane reactor was proposed and investigated experimentally to decrease the reaction temperature of dry reforming to a mid/low temperature range (573 K - 773 K) [8]. The conversion ratio of CH_4 at 673 K and 698 K reached 20.27% and 30.00%, respectively. The thermodynamic analysis on solar CH_4 system reforming with H_2 permeation membrane reactor at mid/low temperature was carried out numerically [9]. A solar trough collector was assumed to provide heat for the CH_4 system reforming. An optimal conversion ratio range of CH_4 for efficient solar CH_4 membrane reforming was calculated, resulting that the net solar-to-fuel efficiency reached 38.25% at 673 K which was lower temperature than normal operation temperature due to non-equilibrium state of CH_4 steam reforming by means of membrane. A reflux solar CH_3OH steam reforming reactor system was proposed and investigated numerically [10]. Parabolic solar collector was adopted to provide the heat for CH_3OH steam reforming. The energy conversion efficiency varied slightly with the inlet mass flow rate. The parabolic trough solar receiver-reactor was proposed and investigated numerically using the CFD software ANSYS Fluent for continuous and efficient H_2 production via CH_3OH steam reforming reaction [11]. A higher working temperature provided a relatively larger energy fraction of thermal loss. The parabolic trough solar receiver reactors of gradually varied porosity catalyst beds were proposed and investigated for cost-efficient H_2 production [12]. A 3D comprehension model was developed for the parabolic trough solar receiver-reactors of CH_3OH steam reforming reaction in porous $Cu/ZnO/Al_2O_3$ catalyst-packed beds, by combining the finite volume method with a comprehensive kinetic model. According to NEDO Renewable Energy Technology White Paper [13], parabolic trough type, Fresnel type, tower type and dish type are main type of concentration solar collectors installed in the world. The efficiency of parabolic trough type, Fresnel type, tower type and dish type is 15%, 8% - 10%, 20% - 35% and 25% - 30%, respectively. Additionally, the land utilization efficiency for parabolic trough type, Fresnel type and tower type is 25% - 40%, 60% - 80% and 20% - 25%, respectively. When using the solar thermal power generation for the plant size below 250 MW and over 250 MW, the power generation cost of parabolic trough type is approximately 0.2 USD/kWh - 0.3 USD/kWh and 0.22 USD/kWh - 0.27 USD/kWh, respectively. Although the power generation cost depends strongly on the sunlight illumination condition in this study, the parabolic trough solar collector was selected for study.

Considering the system proposed by this study, the location where the system is installed is important since the solar intensity influences the performance of solar collector [5]. In addition, the energy consumption and the CO_2 emission in Asia, e.g. China, India, Japan and so on increase rapidly [1]. The average global horizontal solar irradiance in India is 5.0 $kWh/(m^2 \cdot day)$ - 5.5 $kWh/(m^2 \cdot day)$, which is much larger than that in China and Japan, e.g. 3.0 $kWh/(m^2 \cdot day)$ - 4.5 $kWh/(m^2 \cdot day)$ and 3.0 $kWh/(m^2 \cdot day)$ - 3.5 $kWh/(m^2 \cdot day)$, respectively [14]. Therefore, this paper conducted a hypothetical case study by assuming to install the proposed system in Kolkata, India.

However, there is no study on assessment of performance of solar collector as well as the energy production system which is assumed to be installed in India. Therefore, the aim of this study is to understand the influence of the climate data in India on the performance of solar collectors with different sizes and heat mass flow rate of transfer fluid, e.g. the simulated biogas as well as the performance of the combination system proposed. The weather data of Kolkata was from METPV-ASIA [15]. This study used the developed heat transfer model of the parabolic trough solar collector in previous studies [16]. The temperature of heat transfer fluid out of the parabolic trough solar collector could range from approximately 700 K - 873 K [17] [18]. Since the biogas dry reforming could happen in the temperature range from 673 K to 873 K as per the previous experimental studies conducted by authors [19] [20], this study thinks that the parabolic trough solar collector is suitable. The authors have also adopted the specific characteristics of a biogas dry reforming reactor developed previously to calculate the amount of H_2 produced [19] [20] and the power generated by SOFC using H_2 obtained from a biogas dry reforming reactor. The heat transfer fluid which consists of CH_4 and CO_2 flows into the solar collector. After the heat transfer fluid is heated by solar collector, it flows into the biogas dry reforming reactor. H_2 will then be produced in the reactor via the biogas dry reforming process. The produced H_2 is provided to SOFC as a fuel, resulting that the electricity is generated. In this study, the impact of the climate condition of Kolkata in India on the performance of solar collectors with different lengths of parabolic trough solar collector (dx) and mass flow rate of heat transfer fluid (m) has been investigated. In addition, the amount of H_2 produced by biogas dry reforming (G_{H2}), the amount of power generated by SOFC (P_{SOFC}) and the maximum possible households (N) whose electricity demand could be met by the energy system proposed have been also evaluated considering the performance of solar collector with the different dx and m.

2. Heat Transfer Model

2.1. Governing Equations

Figure 1 illustrates the schematic drawing for the simplified heat transfer model of the solar collector proposed in this study. Solar radiation is mainly absorbed on the outer surface of the absorber tube in this model [8]. The absorbed heat transports to the heat transfer fluid by conduction through the tube wall and

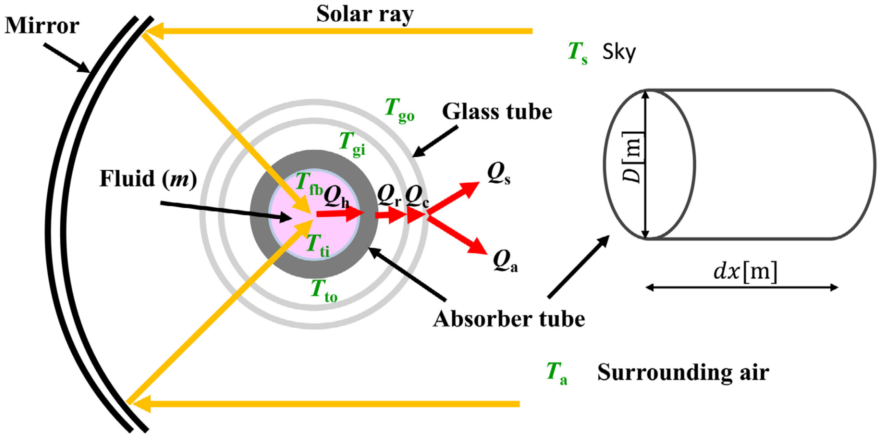

Figure 1. Schematic drawing of heat transfer model of solar collector investigated in this study.

convection from the inner surface of the tube to the fluid (Q_h). Other heat transfers as a radiation loss to the inner surface of the glass tube through the vacuum space (Q_r) and then by conduction from the inner surface of the glass tube to the outer surface of it (Q_c). The heat is transferred to the ambient from the outlet surface of the glass tube via two mechanisms as follows: 1) the convection to the surrounding air (Q_a), 2) the radiation to the sky (Q_s).

Figure 2 exhibits the thermal resistance diagram of the heat transfer process in the model proposed by this study [21]. In this model, R_1 means the thermal resistance because of convection from the heat transfer fluid to the absorber [(m·K)/K]. R_2 means the thermal resistance because of conduction via the absorber [(m·K)/K]. R_3 means the thermal resistance because of radiation via vacuum [(m·K)/K]. R_4 means the thermal resistance because of conduction via the glass tube [(m·K)/K]. R_5 means the thermal resistance because of convection to the surrounding air [(m·K)/K]. R_6 means the thermal resistance because of radiation to the surrounding surfaces (sky) [(m·K)/K].

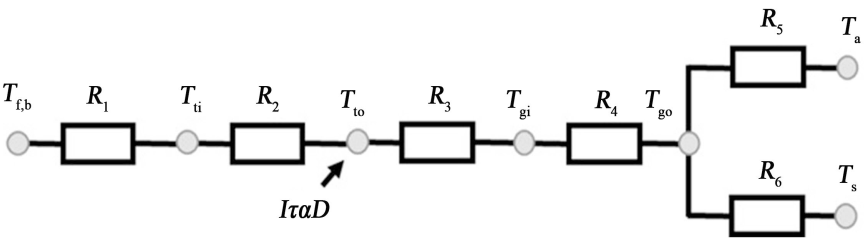

Figure 2. A thermal resistance diagram of the heat transfer model is proposed by this study.

This study assumes the surrounding surface temperature is equal to the ambient air temperature. The model equation for a single glass tube can be expressed as following:

$$I\alpha\tau D\pi dx = \frac{T_{to}-T_{fb}}{R_1} + \frac{T_{to}-T_s}{\left(R_5^{-1}+R_6^{-1}\right)^{-1}} \tag{1}$$

$$mc\frac{dT_{fb}}{dx} = mc\frac{T_{fb,out}-T_{fb,in}}{dx} = \frac{T_{to}-T_{fb}}{R_1} \tag{2}$$

$$\frac{T_{to}-T_{gi}}{R_3} = \frac{T_{to}-T_s}{R_3+\left(R_5^{-1}+R_6^{-1}\right)^{-1}} \tag{3}$$

where I means the solar intensity [W/m^2], α means the absorptivity of absorber tube [−], τ means the transmissivity of glass tube [−], D means the diameter of absorber [m], dx means the length of absorber [m], m means the mass flow rate of heat transfer fluid assumed to be a biogas [kg/s], c means the specific heat of heat transfer fluid [J/(kg·K)], T_{fb} means the temperature of heat transfer fluid [K], $T_{fb,out}$ and $T_{fb,in}$ mean the temperature of heat transfer fluid at outlet [K] and inlet [K], respectively.

Each thermal resistance is defined as the following [16]:

$$R_1 = \frac{1}{2\pi r_{\mathrm{ti}} h} \tag{4}$$

$$R_2 = \frac{1}{2\pi k_{\mathrm{t}}} \ln \frac{r_{\mathrm{to}}}{r_{\mathrm{ti}}} \tag{5}$$

$$R_3 = \frac{1}{2\pi \sigma r_{\mathrm{to}}} \left[\frac{1}{\varepsilon_{\mathrm{t}}} + \frac{1-\varepsilon_{\mathrm{g}}}{\varepsilon_{\mathrm{g}}} \left(\frac{r_{\mathrm{to}}}{r_{\mathrm{gi}}} \right) \right] \left[\left(T_{\mathrm{to}}^2 + T_{\mathrm{gi}}^2 \right) \left(T_{\mathrm{to}} + T_{\mathrm{gi}} \right) \right]^{-1} \tag{6}$$

$$R_4 = \frac{1}{2\pi k_{\mathrm{g}}} \ln \frac{r_{\mathrm{go}}}{r_{\mathrm{gi}}} \tag{7}$$

$$R_5 = \frac{1}{2\pi r_{\mathrm{go}} h_{\mathrm{o}}} \tag{8}$$

$$R_6 = \frac{1}{\varepsilon_{\mathrm{g}} \sigma 2\pi r_{\mathrm{go}} \left(T_{\mathrm{go}} + T_{\mathrm{s}} \right) \left(T_{\mathrm{go}}^2 + T_{\mathrm{s}}^2 \right)} \tag{9}$$

where r_{ti} means the inner radius of absorber [m], r_{to} means the outlet radius of absorber [m], r_{gi} means the inner radius of glass tube [m], r_{go} means the outlet of glass tube [m], σ means Stefan-Boltzmann constant [W/(m^2·K^4)], h means the heat transfer coefficient between the heat transfer fluid and the inner surface of absorber [W/(m^2·K)], h_{o} means the heat transfer coefficient from the outer surface of glass tube to the surrounding air [W/(m^2·K)], k_{t} means the thermal conductivity of absorber [W/(m·K)], k_{g} means the thermal conductivity of glass tube [W/(m·K)], ε_{t} means the emissivity of absorber [−], ε_{g} means the emissivity of glass tube [−], T_{to} means the temperature of outer surface of absorber [−], T_{gi} means the temperature of inner surface of glass tube [K], T_{go} means the temperature of outer surface of glass tube [K], T_{s} means the temperature of sky [K] and T_{a} means the temperature surrounding air (=293) [K]. We assume $T_{\mathrm{s}} \fallingdotseq T_{\mathrm{a}}$.

2.2. Calculation Procedure of Heat Transfer Coefficient

The convective heat transfer coefficient of the turbulent flow in a tube was calculated by Dittus-Boelter correlations [22] in this study as following:

$$Nu = 0.023 Re^{0.8} Pr^{1/3} \tag{10}$$

Additionally, the above equation is summarized in detail which is well known dimensionless number and equation as following:

$$Nu = \frac{hD}{k_{\mathrm{a}}} \tag{11}$$

$$Re = \frac{\rho_{\mathrm{a}} u_{\mathrm{a}} D}{\mu_{\mathrm{a}}} \tag{12}$$

$$Pr = \frac{C_{\mathrm{p,a}} \mu_{\mathrm{a}}}{k_{\mathrm{a}}} \tag{13}$$

$$h_{\mathrm{o}} = 0.0191 + 0.006608 u_{\mathrm{a}} \tag{14}$$

where $C_{\mathrm{p,a}}$ means the specific heat of surrounding air [J/(kg·K)], μ_{a} means the viscosity [Pa·s], k_{a} means the thermal conductivity of surrounding air [W/(m·K)], u_{a}

means the velocity of surrounding air [m/s] and ρ_a means the density of surrounding air [m/s]. From the reference [16], the temperature of fluid flowing through the absorber was calculated well using the h_o equation shown in Equation (14). Consequently, the authors think the h_o equation shown by Equation (14) can be applied.

2.3. Calculation Procedure of T_{fb}

According to Equations (1) and (2), the following equation can be drawn:

$$T_{\mathrm{fb,out}} = \frac{dx}{mc}\left\{ I\alpha\tau D\pi dx - \frac{\left(T_{\mathrm{to}} - T_{\mathrm{s}}\right)\left(R_5 + R_6\right)}{R_3\left(R_5 + R_6\right) + R_5 R_6} \right\} + T_{\mathrm{fb,in}} \tag{15}$$

Moreover, R_3 can be decided from Equation (3) as following:

$$R_3 = \frac{\left(T_{\mathrm{to}} - T_{\mathrm{gi}}\right) R_5 R_6}{\left(R_5 + R_6\right)\left(-T_{\mathrm{s}} + T_{\mathrm{gi}}\right)} \tag{16}$$

According to Equations (6) and (16), T_{to} can be obtained as following:

$$T_{\mathrm{to}} = \left[\frac{\left(R_5 + R_6\right)\left(-T_{\mathrm{s}} + T_{\mathrm{g}}\right)}{2\pi\sigma t_{\mathrm{to}} R_5 R_6} \times \frac{r_{\mathrm{gi}} + r_{\mathrm{to}}\left(1 - \varepsilon_{\mathrm{g}}\right)}{\varepsilon_{\mathrm{t}} r_{\mathrm{gi}}} + T_{\mathrm{gi}}^4 \right]^{\frac{1}{4}} \tag{17}$$

T_{fb} can be calculated by averaging $T_{fb,\,in}$ and $T_{fb,\,out}$ as following:

$$T_{\mathrm{fb}} = \frac{T_{\mathrm{fb,in}} + T_{\mathrm{fb,out}}}{2} \tag{18}$$

T_{fb} is calculated with changing dx according to the above equations in this study. D was set to be 1.5 m, according to the previous study [5]. The weather data, *i.e.* I, u_a and T_a in Kolkata from METPV-ASIA [15] were used. In this study, the mirror and solar reflection as well as to consider the variable angle and solar radiation were ignored [21]. The heat transfer fluid was a mixture of CH_4 and CO_2. The molar ratio of CH_4:CO_2 was 1.5:1. The following assumptions were made in this study [21]:

1) The distance between the absorber and glass tube is 1/10 D.

2) $T_{fb,\,in}$ is 283 K.

3) $T_{\mathrm{s}} \fallingdotseq T_{\mathrm{a}}$.

4) The thickness of absorber and glass tube is 0.005 m and 0.010 m, respectively.

5) R_2 and R_4 are ignored since they are very small compared with the other thermal resistances.

6) T_{ti} equals to T_{to}.

7) T_{gi} equals to T_{go}, which is 373 K.

8) The mirror and solar reflection is ignored.

9) The variable angle of solar radiation is ignored.

Table 1 lists the physical properties which were used in this study. Before the calculation of T_{fb}, we could not predict the exact value of it. If we calculate T_{fb} considering the change of physical properties with the temperature under an unsteady state condition, the calculation is too complex and huge. The physical properties listed in **Table 1** were assumed to be temperature-independent, and the values of 283 K were listed and used.

Comparing the other heat transfer models, a few papers reported on the heat transfer analysis using Hottel-Whiller-Bliss model for a solar collector recently [23]-[25]. However, these papers investigated on a flat plate solar collector [23]-[25], while this study investigates a parabolic trough solar collector. Moreover, the Hotel-Whiller-Bliss model considered thermal conduction only in these previous studies [23]-[25], while this model investigated in this study considers the thermal conduction, the thermal convection and the thermal radiation heat transfer, resulting in the assessment of the whole heat transfer mechanism in this study. Consequently, the authors think the model investigated in this study has the merit and the superiority to Hottel-Whiller-Bliss model.

Table 1. The physical properties adopted in this study are [5] [16] [21].

Property	Value	Information
α [−]	0.94	-
τ [−]	0.94	-
ε_t [−]	0.9	-
c [J/(kg·K)]	1.335	for CH_4:CO_2 = 1.5:1
σ [W/(m^2·K^4)]	5.67×10^{-8}	Stefan-Boltzmann coefficient
ε_g [−]	0.94	Glass smooth surface
k_a [W/(m·K)]	0.0257	Surrounding air
ρ_a [kg/m^3]	1.166	Surrounding air
μ_a [Pa·s]	1.82×10^{-5}	Surrounding air
$C_{p,a}$ [J/(kg·K)]	1006	Surrounding air
k_t [W/(m·K)]	16	Stainless steel
K_g [W/(m·K)]	1.3	Quartz glass

3. Combined Energy Production System

Figure 3 illustrates the proposed systems consisting of solar collector, biogas dry reforming reactor and SOFC. In the proposed system, the heat transfer fluid which consists of CH_4 and CO_2 flows into solar collector. After being heated by solar collector, the heat transfer fluid flows into biogas dry reforming reactor. H_2 is produced in the reactor via biogas dry reforming process. The produced H_2 is supplied as fuel for SOFC. As a result, the electricity and heat is generated (In this study, only the electricity is considered). The by-product of the process, CO was not considered in this study. Generally, a biogas is used as a fuel for a micro gas turbine and a gas engine [4]. The power generation efficiency of micro gas turbine and gas engine is 33% [26], and approximately 30% [27], respectively. On the other hand, as to the combination system proposed by this study, the power generation efficiency of SOFC is 55% [28]. In addition, SOFC can be used as a co-generation system whose energy conversion efficiency is 87% [29]. Therefore, the system proposed by this study has a superiority to the existing system using a biogas as a fuel.

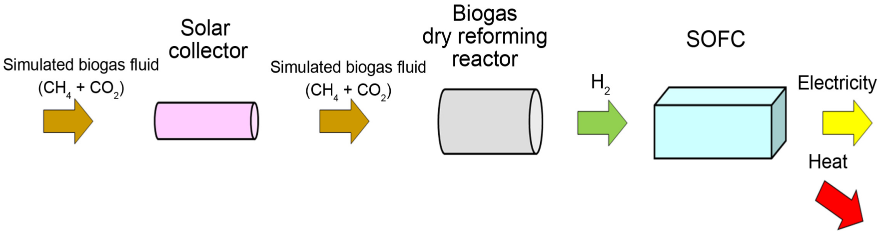

Figure 3. Combined energy production system consisting of solar collector, biogas dry reforming reactor and SOFC proposed by this study.

To calculate the amount of H_2 produced through the biogas dry reforming reactor, this study follows the reaction scheme of biogas dry reforming as follows:

$$CH_4 + CO_2 \rightarrow 2H_2 + 2CO \tag{19}$$

We set the molar ratio of CH_4 and CO_2 is 2.51 × 10^3 mol/s and 1.67 × 10^3 mol/s, respectively when m = 0.005 kg/s. In this study, m is changed by 0.005, 0.010, 0.015 and 0.030 kg/s. According to Equation (19) and the molar flow rate when m = 0.005 kg/s, the molar flow rate of produced H_2 can be estimated to be 3.34 × 10^{-3} mol/s. According to the authors' previous experimental studies investigating the impact of the reaction temperature on the performance of biogas dry reforming corresponding to T_{fb} in this study from 673 K to 873 K [19] [20], the best performance of biogas dry reforming was obtained at 873 K. The conversion ratio of H_2 is assumed to be 100% and 10% respectively [19] [20].

To calculate the power generated by SOFC, the lower heating value of H_2 (=10.79 MJ/m^3N) and the power generation efficiency commercial SOFC of 55% [28] were used. The power generated by SOFC in the case of the conversion ratio of H_2 = 100% can be estimated as follows:

$$\begin{aligned}&\left(3.34\times10^{-3}\left[\text{mol/s}\right]\times22.4\left[\text{L/mol}\right]\right)\\&\div\left(1000\left[\text{L/m}^3\right]\times0.55\times10.79\left[\text{MJ}/\left(\text{m}^3\cdot\text{N}\right)\right]\right)=0.444\left[\text{kW}\right]\end{aligned}$$

In addition, this study estimated the number of maximum possible households whose electricity demand could be met by the power generated by SOFC. The monthly data for the electricity demand of a couple households was used in this study [30].

4. Results and Discussion

4.1. Change of T_{fb} through Year with Different dx and m

The climate data, I, u_a and T_a in Kolkata, India according to METPV-ASIA [15] were used for the calculation of T_{fb}, and are shown in **Tables 2-14**.

Figures 4-15 show the changes of T_{fb} with time in different months. In these

Table 2. Climate data of I, u_a and T_a in Kolkata, India in January.

Time	I [MJ/m^2]	u_a [m/s]	T_a [K]
7:00	0.087	0.258	287.02
8:00	0.498	0.323	287.02
9:00	0.877	1.000	294.94
10:00	1.271	1.000	294.94
11:00	1.576	1.000	294.94
12:00	1.725	1.000	294.94
13:00	1.666	1.000	294.94
14:00	1.413	0.935	294.94
15:00	1.134	0.194	293.85
16:00	0.935	0.194	293.85
17:00	0.389	0.194	293.85
18:00	0.003	0.194	293.85

Table 3. Climate data of I, u_a and T_a in Kolkata, India in February.

Time	I [MJ/m^2]	u_a [m/s]	T_a [K]
7:00	0.162	0.214	289.65
8:00	0.700	0.214	289.65
9:00	1.173	0.214	299.87
10:00	1.674	0.964	299.87
11:00	1.966	0.964	299.87
12:00	2.124	0.964	299.87
13:00	2.085	0.964	299.87
14:00	1.830	0.964	299.87
15:00	1.508	0.214	298.80
16:00	1.282	0.214	298.80
17:00	0.660	0.214	298.80
18:00	0.090	0.214	298.80

Table 4. Climate data of I, u_a and T_a in Kolkata, India in March.

Time	I [MJ/m^2]	u_a [m/s]	T_a [K]
7:00	0.406	0.548	295.34
8:00	1.000	0.548	295.34
9:00	1.534	1.065	304.23
10:00	2.012	1.065	304.23
11:00	2.364	1.065	304.23
12:00	2.565	1.065	304.23
13:00	2.505	1.065	304.23
14:00	2.255	1.065	304.23
15:00	1.816	0.581	303.07
16:00	1.199	0.581	303.07
17:00	0.681	0.581	303.07

18:00	0.108	0.581	303.07

Table 5. Climate data of I, u_a and T_a in Kolkata, India in April.

Time	I [MJ/m^2]	u_a [m/s]	T_a [K]
7:00	0.643	0.867	298.37
8:00	1.163	0.867	298.37
9:00	1.657	1.600	305.65
10:00	2.092	1.600	305.65
11:00	2.433	1.600	305.65
12:00	2.672	1.600	305.65
13:00	2.581	1.600	305.65
14:00	2.323	1.600	305.65
15:00	1.844	1.333	304.17
16:00	1.239	1.333	304.17
17:00	0.744	1.333	304.17
18:00	0.158	1.333	304.17

Table 6. Climate data of I, u_a and T_a in Kolkata, India in May.

Time	I [MJ/m^2]	u_a [m/s]	T_a [K]
7:00	0.744	0.355	299.41
8:00	1.266	0.355	299.41
9:00	1.771	1.290	306.59
10:00	2.223	1.290	306.59
11:00	2.555	1.290	306.59
12:00	2.684	1.290	306.59
13:00	2.555	1.290	306.59
14:00	2.241	1.290	306.59
15:00	1.786	1.613	304.59
16:00	1.150	1.613	304.49
17:00	0.517	1.613	304.49
18:00	0.184	1.613	304.49

Table 7. Climate data of I, u_a and T_a in Kolkata, India in June.

Time	I [MJ/m^2]	u_a [m/s]	T_a [K]
7:00	0.651	1.033	300.15
8:00	1.029	1.033	300.15
9:00	1.552	1.367	305.26
10:00	1.939	1.367	305.26
11:00	2.191	1.367	305.26
12:00	2.187	1.367	305.26
13:00	2.046	1.367	305.26
14:00	1.729	1.367	305.26
15:00	1.138	1.200	302.89
16:00	0.722	1.200	302.89
17:00	0.302	1.200	302.89

18:00	0.133	1.200	302.89

Table 8. Climate data of I, u_a and T_a in Kolkata, India in July.

Time	I [MJ/m^2]	u_a [m/s]	T_a [K]
7:00	0.556	0.484	300.25
8:00	0.926	0.484	300.25
9:00	1.260	1.452	304.60
10:00	1.579	1.452	304.60
11:00	1.796	1.452	304.60
12:00	1.828	1.452	304.60
13:00	1.792	1.452	304.60
14:00	1.538	1.452	304.60
15:00	1.390	1.097	303.29
16:00	1.504	1.097	303.29
17:00	0.997	1.097	303.29
18:00	0.454	1.097	303.29

Table 9. Climate data of I, u_a and T_a in Kolkata, India in August.

Time	I [MJ/m^2]	u_a [m/s]	T_a [K]
7:00	0.586	0.645	300.31
8:00	1.037	2.032	300.31
9:00	1.434	2.032	305.28
10:00	1.871	2.032	305.28
11:00	2.133	2.032	305.28
12:00	2.155	2.032	305.28
13:00	1.874	2.032	305.28
14:00	1.614	2.032	305.28
15:00	1.346	1.323	302.75
16:00	0.844	1.323	302.75
17:00	0.444	1.323	302.75
18:00	0.143	1.323	302.75

Table 10. Climate data of I, u_a and T_a in Kolkata, India in September.

Time	I [MJ/m^2]	u_a [m/s]	T_a [K]
7:00	0.518	0.333	299.56
8:00	0.972	0.333	299.56
9:00	1.409	1.267	304.88
10:00	1.775	1.267	304.88
11:00	1.981	1.267	304.88
12:00	2.019	1.267	304.88
13:00	1.901	1.267	304.88
14:00	1.645	1.267	304.88
15:00	1.178	1.033	302.16
16:00	0.622	1.033	302.16
17:00	0.338	1.033	302.16

18:00	0.040	1.033	302.16

Table 11. Climate data of I, u_a and T_a in Kolkata, India in October.

Time	I [MJ/m^2]	u_a [m/s]	T_a [K]
7:00	0.476	0.290	298.05
8:00	0.968	0.290	298.05
9:00	1.404	1.097	303.70
10:00	1.773	1.097	303.70
11:00	2.025	1.097	303.70
12:00	2.100	1.097	303.70
13:00	1.924	1.097	303.70
14:00	1.594	1.097	307.70
15:00	1.203	0.613	300.89
16:00	0.621	0.613	300.89
17:00	0.221	0.613	300.89
18:00	6.452×10^{-4}	0.613	300.89

Table 12. Climate data of I, u_a and T_a in Kolkata, India in November.

Time	I [MJ/m^2]	u_a [m/s]	T_a [K]
7:00	0.340	0.333	292.90
8:00	0.863	0.367	292.90
9:00	1.345	1.133	301.10
10:00	1.749	1.133	301.10
11:00	2.038	1.133	301.10
12:00	2.075	1.133	301.10
13:00	1.942	1.133	301.10
14:00	1.613	1.100	301.10
15:00	1.119	0.267	297.87
16:00	0.680	0.267	297.87
17:00	0.158	0.267	297.87
18:00	0	3.597	297.87

Table 13. Climate data of I, u_a and T_a in Kolkata, India in December.

Time	I [MJ/m^2]	u_a [m/s]	T_a [K]
7:00	0.170	0.168	287.07
8:00	0.676	0.181	287.07
9:00	1.118	0.945	298.35
10:00	1.502	0.971	298.35
11:00	1.760	1.087	298.35
12:00	1.850	1.023	298.35
13:00	1.755	1.003	298.35
14:00	1.504	0.977	298.35
15:00	1.085	0.094	294.41
16:00	0.668	0.071	294.41
17:00	0.163	0.097	294.41

18:00	0	0.142	294.41

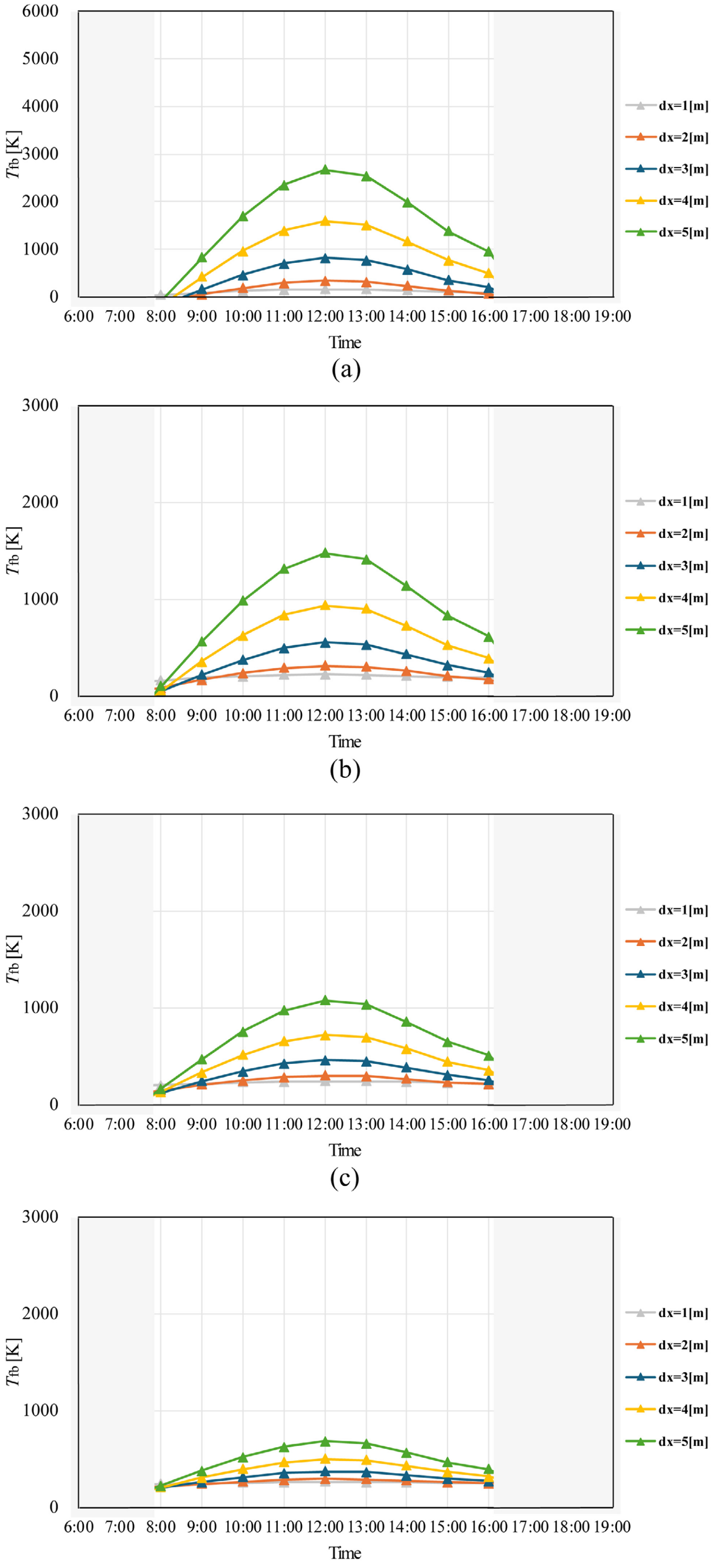

(d)

Figure 4. Comparison of change of T_{fb} with time among different *dx* and

m in January ((a): m = 0.005 kg/s, (b): m = 0.010 kg/s, (c): m = 0.015 kg/s, (d): m = 0.030 kg/s).

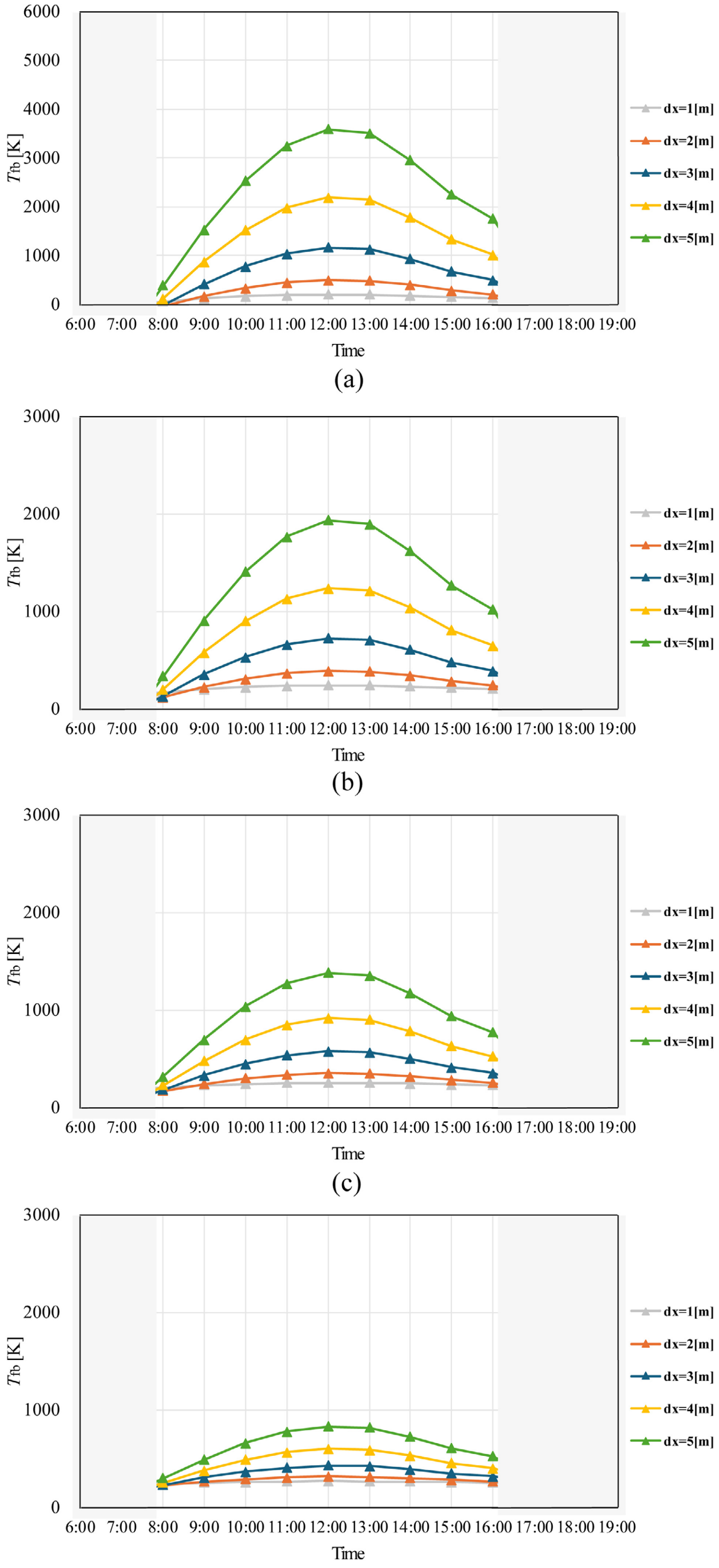

(a)

(b)

(c)

(d)

Figure 5. Comparison of change of T_{fb} with time among different dx and m

in February ((a): m = 0.005 kg/s, (b): m = 0.010 kg/s, (c): m = 0.015 kg/s, (d): m = 0.030 kg/s).

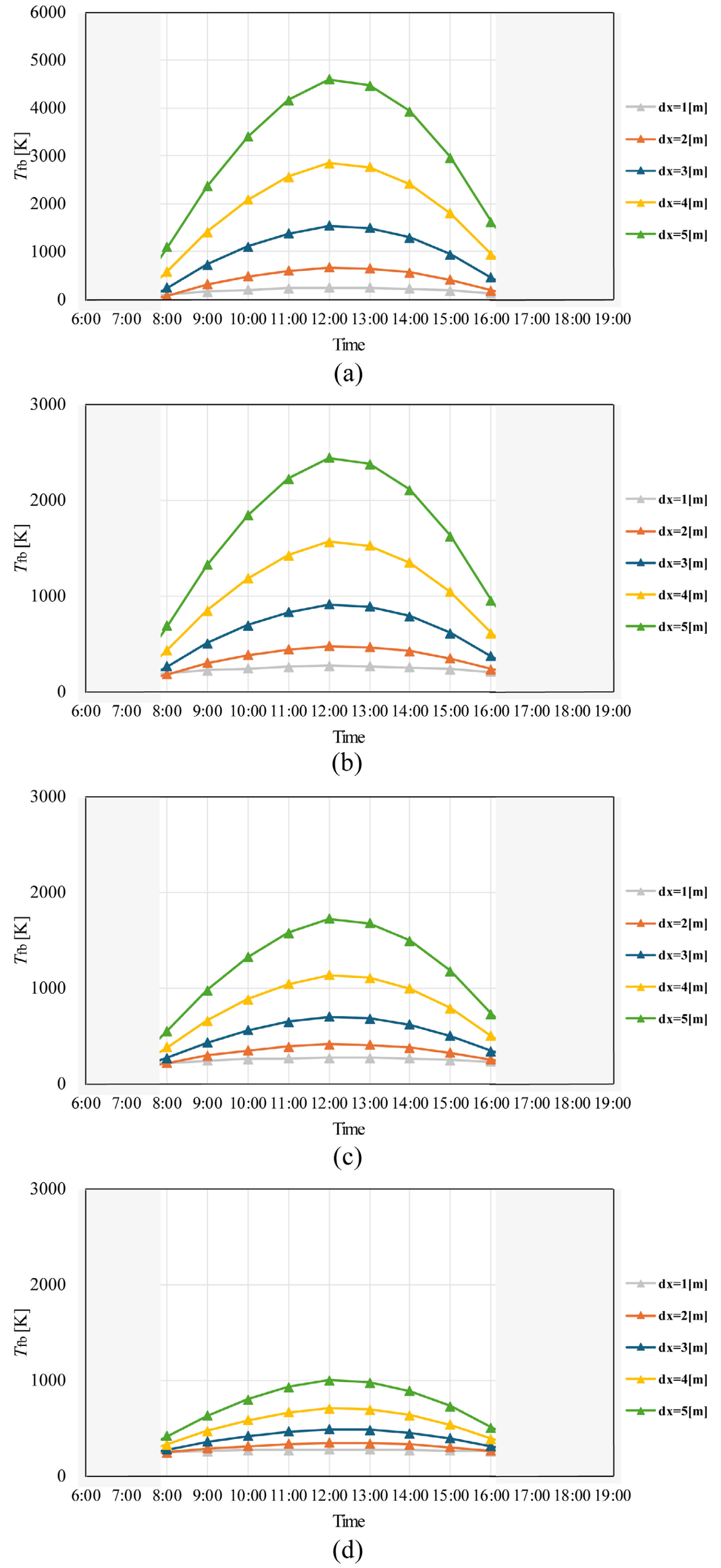

Figure 6. Comparison of change of T_{fb} with time among different dx and m

in March ((a): m = 0.005 kg/s, (b): m = 0.010 kg/s, (c): m = 0.015 kg/s, (d): m = 0.030 kg/s).

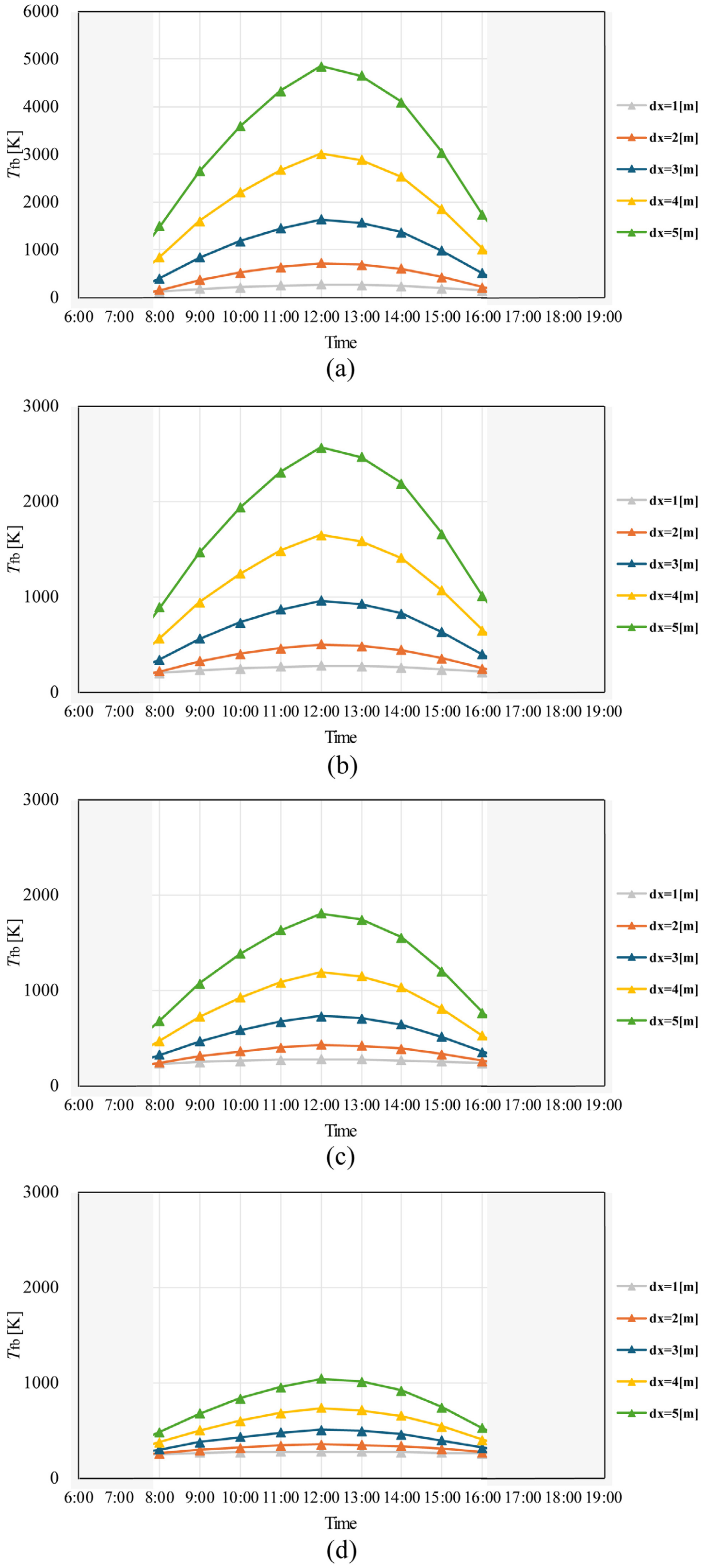

(a)

(b)

(c)

(d)

Figure 7. Comparison of change of T_{fb} with time among different dx and

m in April ((a): m = 0.005 kg/s, (b): m = 0.010 kg/s, (c): m = 0.015 kg/s, (d): m = 0.030 kg/s).

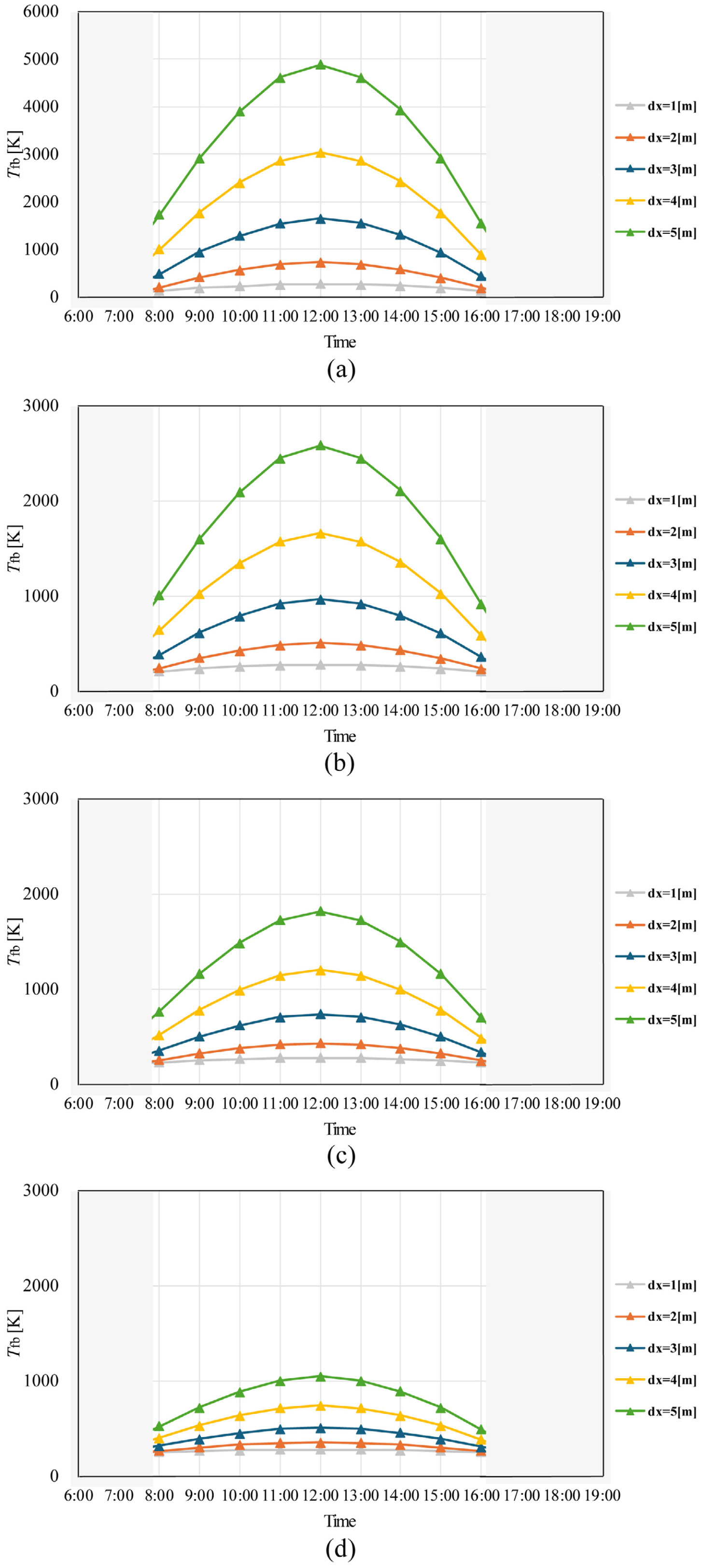

(a)

(b)

(c)

(d)

Figure 8. Comparison of change of T_{fb} with time among different dx and

m in May ((a): $m = 0.005$ kg/s, (b): $m = 0.010$ kg/s, (c): $m = 0.015$ kg/s, (d): $m = 0.030$ kg/s).

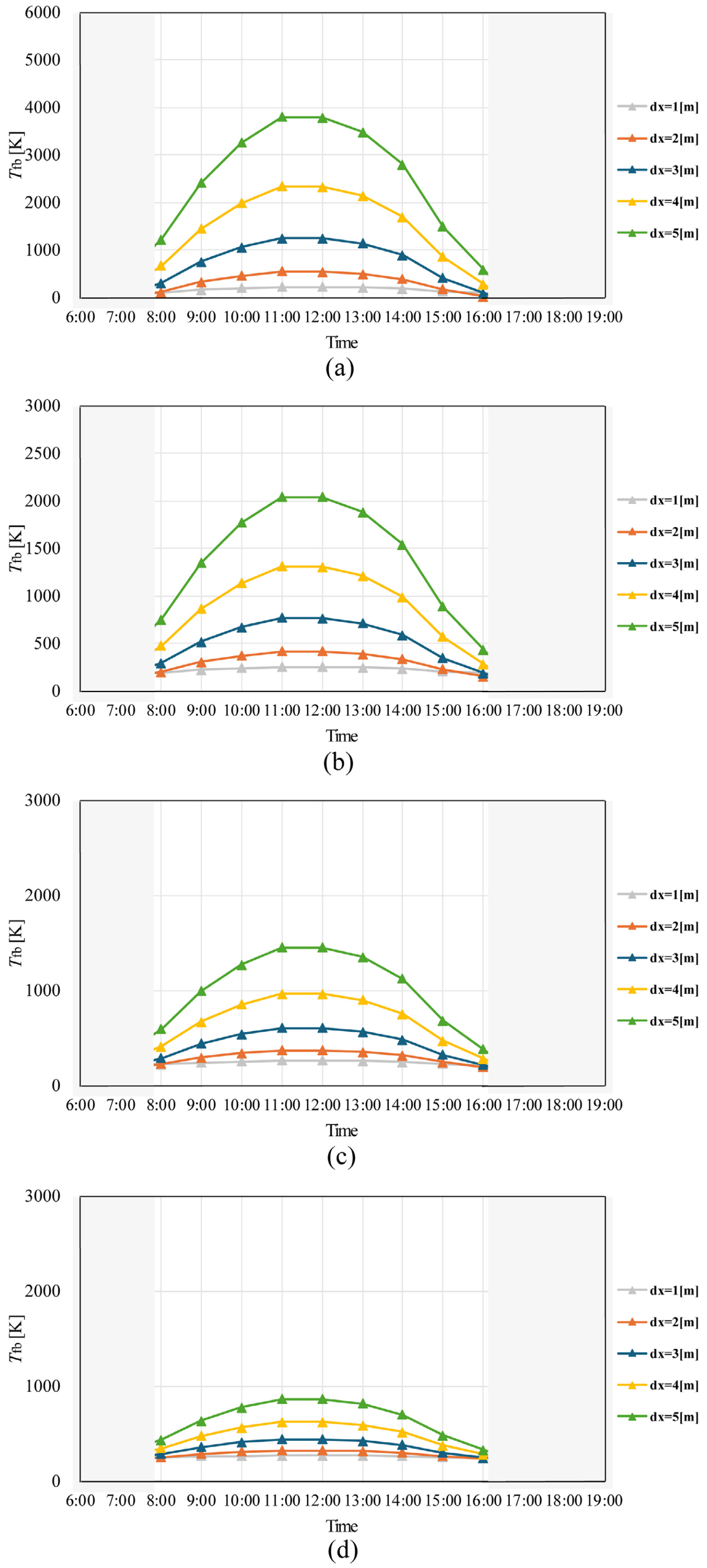

Figure 9. Comparison of change of T_{fb} with time among different dx and

m in June ((a): $m = 0.005$ kg/s, (b): $m = 0.010$ kg/s, (c): $m = 0.015$ kg/s, (d): $m = 0.030$ kg/s).

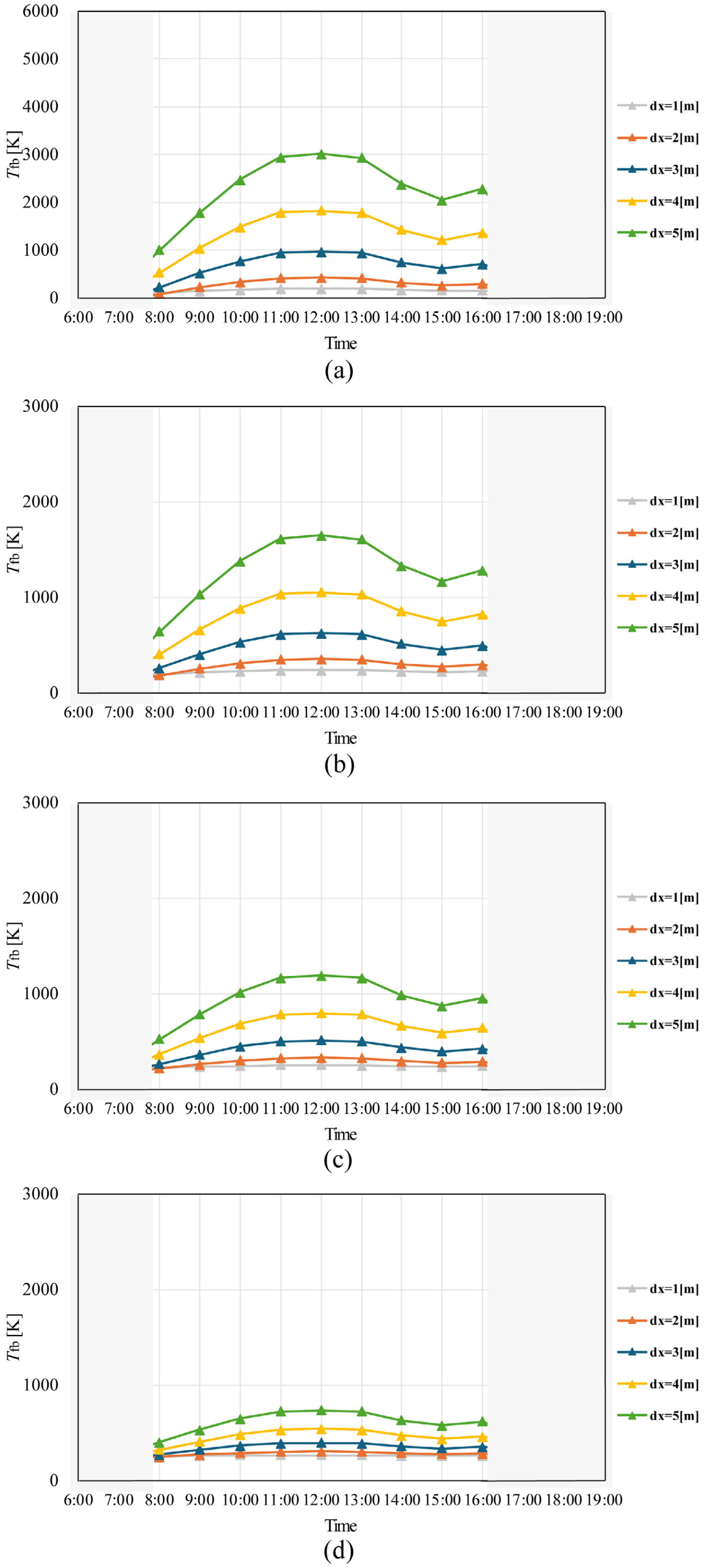

(a)

(b)

(c)

(d)

Figure 10. Comparison of change of T_{fb} with time among different dx and

m in July ((a): m = 0.005 kg/s, (b): m = 0.010 kg/s, (c): m = 0.015 kg/s, (d): m = 0.030 kg/s).

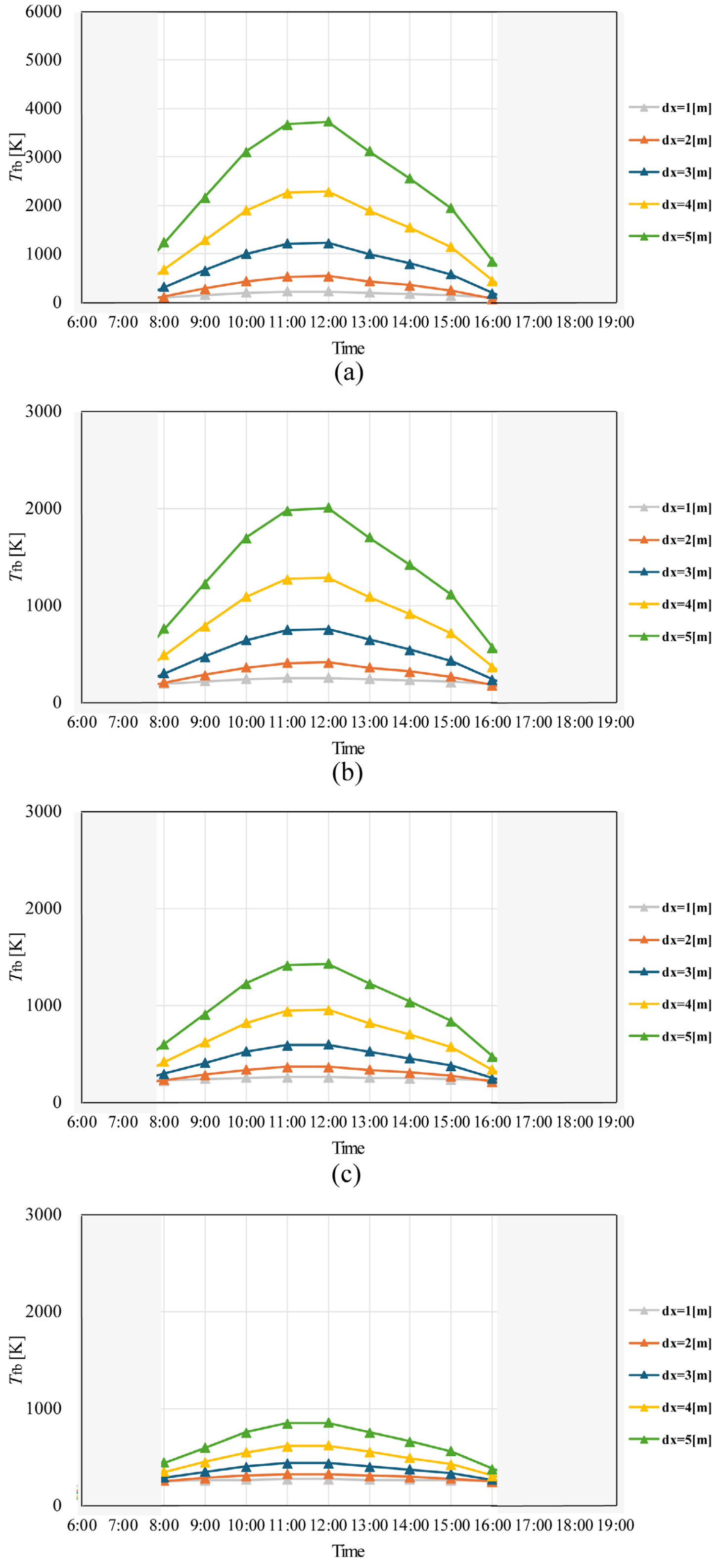

Figure 11. Comparison of change of T_{fb} with time among different dx and

m in August ((a): m = 0.005 kg/s, (b): m = 0.010 kg/s, (c): m = 0.015 kg/s, (d): m = 0.030 kg/s).

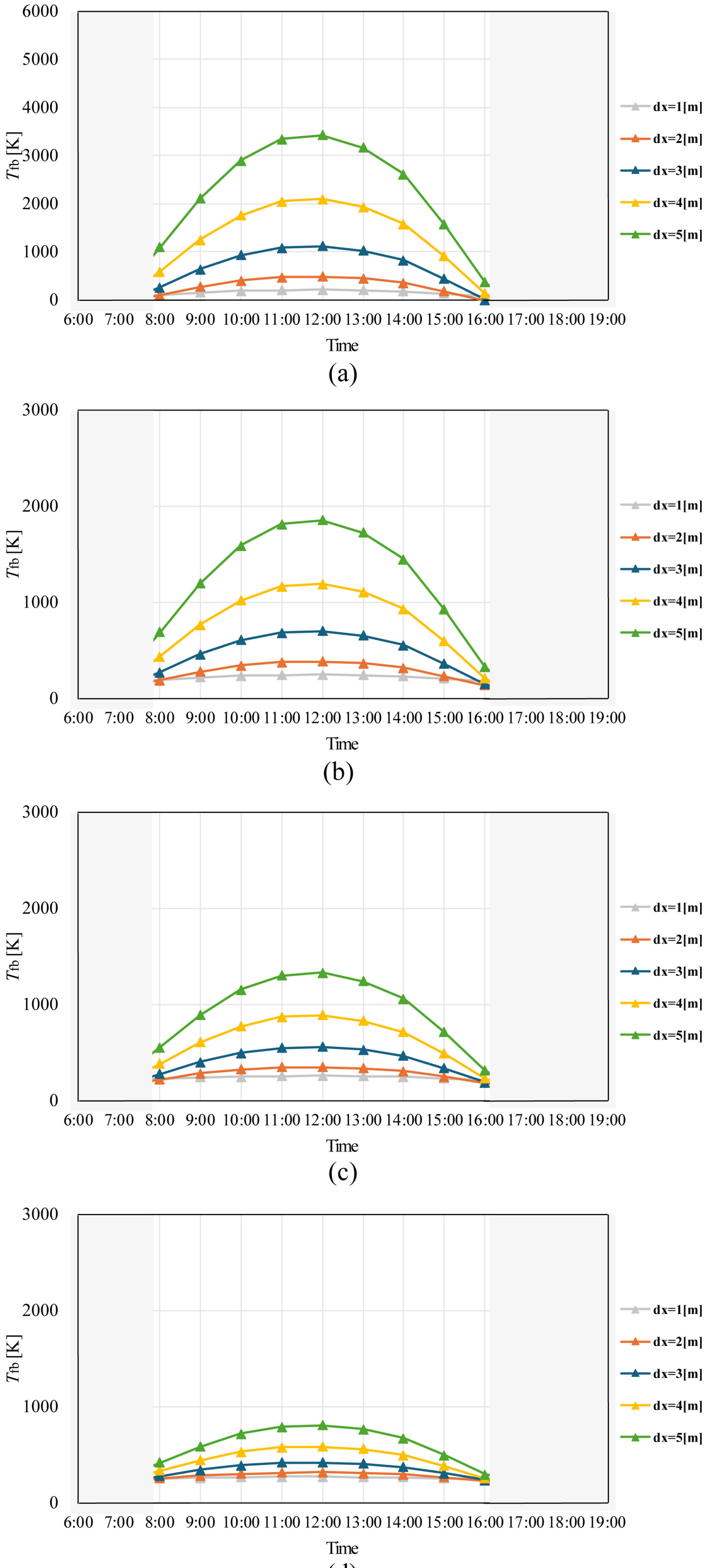

(a)

(b)

(c)

(d)

Figure 12. Comparison of change of T_{fb} with time among different dx and

m in September ((a): m = 0.005 kg/s, (b): m = 0.010 kg/s, (c): m = 0.015 kg/s, (d): m = 0.030 kg/s).

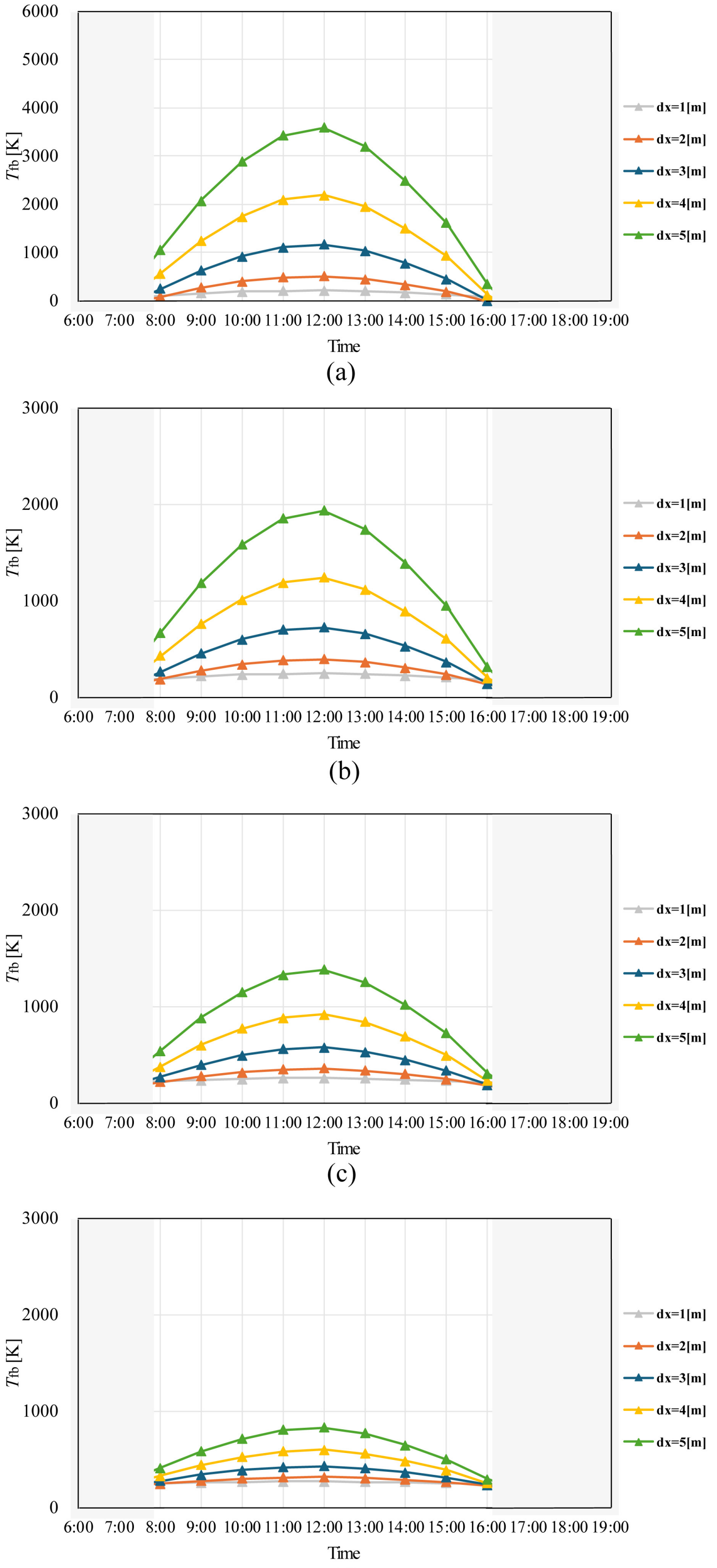

(a)

(b)

(c)

(d)

Figure 13. Comparison of change of T_{fb} with time among different dx and

m in October ((a): $m = 0.005$ kg/s, (b): $m = 0.010$ kg/s, (c): $m = 0.015$ kg/s, (d): $m = 0.030$ kg/s).

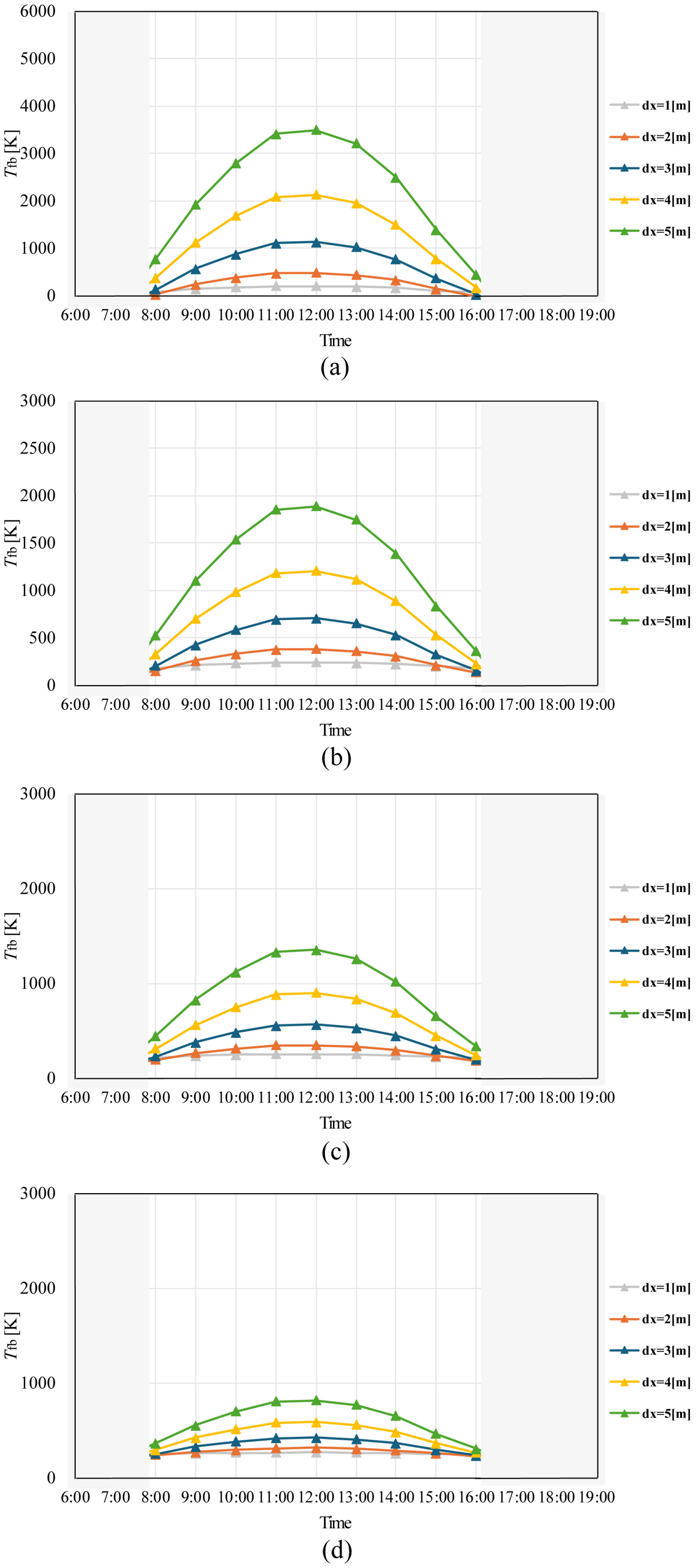

(a)

(b)

(c)

(d)

Figure 14. Comparison of change of T_{fb} with time among different dx and

m in November ((a): m = 0.005 kg/s, (b): m = 0.010 kg/s, (c): m = 0.015 kg/s, (d): m = 0.030 kg/s).

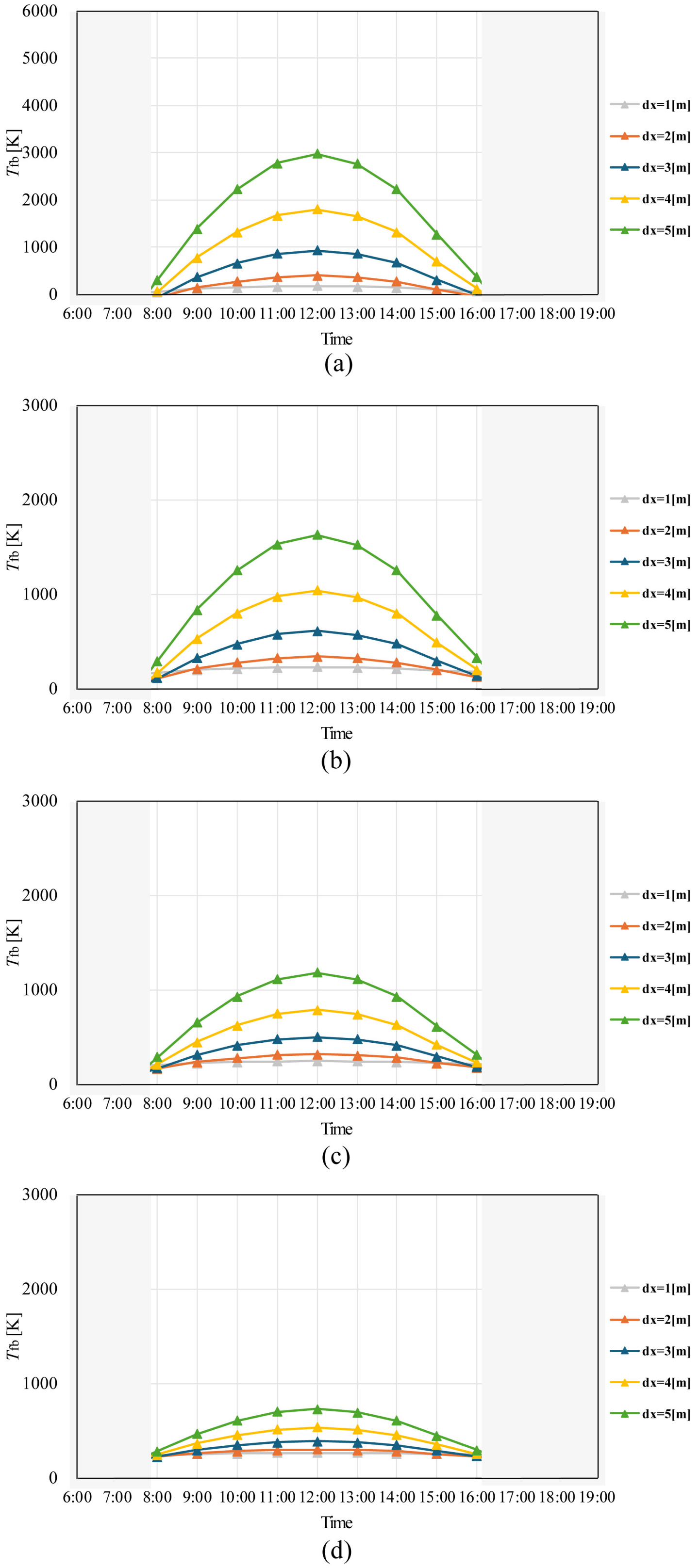

(a)

(b)

(c)

(d)

Figure 15. Comparison of change of T_{fb} with time among different dx and

m in December ((a): m = 0.005 kg/s, (b): m = 0.010 kg/s, (c): m = 0.015 kg/s, (d): m = 0.030 kg/s).

figures, dx and m were also changed. The monthly mean values are shown in these figures. According to **Tables 2-13** and **Figures 4-15**, the change in T_{fb} followed the change in I mainly. Additionally, it can also be seen from **Figures 4-15** that T_{fb} rises with the increase in dx. This is due to the increase in heat transfer area for receiving the solar heat, which can be understood from Equation (15) [21]. However, some conditions exhibited T_{fb} over 2000 K in the case of dx = 5 m, indicating that it was not practically possible due to the durability of material of solar collector. For example, the melting point of SUS 405 is 1700 K [31]. In the following discussion, the results were based on dx = 4 m. In addition, it is shown from **Figures 4-15** that T_{fb} decreases with the increase in m. Since the heat capacity is larger with the increase in m as shown in Equation (15), T_{fb} decreases with the increase in m. It can be found that T_{fb} is below 1000 K even dx = 5 m for some months. Moreover, it can be seen that T_{fb} in March, April and May is higher than the other months. In India, March, April and May belongs to a summer season which exhibits longer sunshine duration and higher I, resulting from **Tables 2-13**. On the other hand, it can be seen from **Figures 4-15** that T_{fb} from June to December is lower than the other months. Since June to December is the rainy season in Kolkata, T_{fb} is lower due to lower I. Therefore, it can be revealed that T_{fb} is determined by the climate characteristics.

4.2. Estimation of H_2 Produced by Biogas Dry Reforming and Power Generation by SOFC

This study assumed that H_2 can be produced by biogas dry reforming when T_{fb} is over 873 K. **Tables 14-17** list G_{H2}, P_{SOFC} and N per month changing m at dx = 4 m according to the duration when T_{fb} is over 873 K shown in **Figures 4-15**.

Table 14. Comparison of G_{H2}, P_{SOFC} and N among different months for m = 0.005 kg/s at dx = 4 m.

	G_{H2} [kg]	P_{SOFC} [Wh]	N [-]
January	4.48	82,639	0.5
February	5.39	99,522	0.7
March	5.97	110,185	0.7
April	6.50	119,959	0.8
May	6.71	123,958	0.8
June	5.78	106,631	0.7
July	5.97	110,185	0.7
August	5.97	110,185	0.7
September	5.05	93,302	0.6
October	5.22	96,412	0.6
November	5.05	93,302	0.6

December	5.22	96,412	0.6
Total	67.31	1,242,691	8.04

Table 15. Comparison of G_{H2}, P_{SOFC} and N among different months for m = 0.010 kg/s at dx = 4 m.

	G_{H2} [kg]	P_{SOFC} [Wh]	N [-]
January	7.46	137,731	0.9
February	9.43	174,163	1.2
March	11.94	220,370	1.4
April	11.55	213,261	1.4
May	11.94	220,370	1.4
June	8.66	159,946	1.0
July	11.94	220,370	1.4
August	10.44	192,824	1.2
September	8.66	159,946	1.0
October	10.44	192,824	1.2
November	8.66	159,946	1.0
December	7.46	137,731	0.9
Total	118.59	2,189,481	14.2

Table 16. Comparison of G_{H2}, P_{SOFC} and N among different months for m = 0.015 kg/s at dx = 4 m.

	G_{H2} [kg]	P_{SOFC} [Wh]	N [-]
January	6.71	123,958	0.8
February	12.13	223,924	1.6
March	15.67	289,235	1.8
April	15.16	279,905	1.8
May	15.67	289,235	1.8
June	12.99	239,919	1.6
July	13.43	247,916	1.6
August	13.43	247,916	1.6
September	12.99	239,919	1.6
October	13.43	247,916	1.6
November	10.83	199,932	1.3
December	11.19	206,597	1.3
Total	153.63	2,836,374	18.35

It can be seen from **Tables 14-17** that G_{H2}, P_{SOFC} and N in March, April and May were higher than that in the other months irrespective of m. The durations when T_{fb} was over 873 K in March, April and May were longer than that in the other months since I_s in March, April and May were higher. In addition, G_{H2}, P_{SOFC} and N increased when m mas larger. Since the mass of simulated biogas, e.g.

heat transfer fluid increased, G_{H2} was larger, causing larger P_{SOFC} and N. However, G_{H2}, P_{SOFC} and N decreased if m was set over 0.05 kg/s. This was due to the increase in heat capacity with the increase in m as shown in Equation (15). Therefore, this study has concluded that the optimum m should be 0.03 kg/s. If the conversion ratio of H_2 is assumed to be 10%, G_{H2}, P_{SOFC} and N become one-tenth compared to each value shown in **Tables 14-17**.

Table 17. Comparison of G_{H2}, P_{SOFC} and N among different months for $m = 0.030$ kg/s at $dx = 4$ m.

	G_{H2} [kg]	P_{SOFC} [Wh]	N [-]
January	0	0	0
February	4.04	74,611	0.5
March	17.90	330,555	2.1
April	21.66	399,865	2.6
May	22.38	413,194	2.6
June	8.66	159,946	1.0
July	0	0	0
August	8.95	165,277	1.0
September	0	0	0
October	4.48	82,639	0.5
November	0	0	0
December	0	0	0
Total	88.07	1,626,116	10.48

Considering N, it is not sufficient to cover the citizen living in Kolkata. However, this study thinks the following approach is efficient:

1) Increase the number of proposed system

2) Increase D and re-optimize the size of solar collector

3) Concentrate the solar light with installing the equipment in order to increase the solar intensity

This study would like to investigate these subjects in the near future.

4.3. Discussion of Result Obtained by This Study and Comparison of It with the Other Researches

This study has revealed that the optimal dx is 4 m due to the durability of the material of solar collector if we install the proposed system in India. In addition, this study has also revealed that the optimal m is 0.03 kg/s. If we can develop a material that can be used over 1700 K, the larger solar collector can be available. In addition, this study has assumed H_2 can be produced by biogas dry reforming when T_{fb} is over 873 K. If the heat with T_{fb} over 873 K can be stored and used in the time or the day with T_{fb} below 873 K, H_2 can be produced more, resulting that P_{SOFC} and N become larger. This study proposes that the biogas heated over 873 K is stored in an adiabatic tank and used for the time when the heat is needed. If this proposal can be realized, the system proposed by this study would be available for wider area and climate conditions.

On the other hand, there is no study on assessment of performance of solar collector as well as the energy production system which is assumed to be installed in India. According to the other researches investigating the solar collector which utilized the obtained for a chemical reaction, the relationship between the conversion ratio of CH_4 and CO_2 and the temperature of heated biogas was reported [7]-[9]. However, this study has assumed that the conversion ratio of H_2, which is similar to the conversion ratio of CH_4, is constant. In addition, this study has revealed that P_{SOFC} and N, which have not been reported in the other researches. Moreover, this finding as well as the performance of solar collector are available for India, which has also not been reported in the other researches. Consequently, the results obtained by this study is meaningful.

5. Conclusions

This study simulated the performances of solar collectors with different dx and m and the energy system proposed with the weather condition in Kolkata, India. In addition, this study evaluated G_{H2}, P_{SOFC}, and N. As a result, the optimum dx was founded to be 4 m considering the melting point of material of solar collector. It is revealed that T_{fb} decreases with the increase in m. In addition, T_{fb} in March, April and May are higher than that in other months since March, April and May are summer in India. On the other hand, T_{fb} from June to December were lower due to the rainy season. As to G_{H2}, P_{SOFC} and N, they were all higher in March, April and May than in other months irrespective of m. Finally, this study reveals that the optimum m is around 0.030 kg/s.

Conflicts of Interest

The authors declare no conflicts of interest regarding the publication of this paper.

References

[1] Agency for Natural Resources and Energy (2024) Energy White Paper 2024. https://www.enecho.meti.go.jp/about/whitepaper/2024/pdf/2_2.pdf

[2] Jelle, B. (2015) Building Integrated Photovoltaics: A Concise Description of the Current State of the Art and Possible Research Pathways. *Energies*, **9**, Article 21. https://doi.org/10.3390/en9010021

[3] World Bioenergy Association (2024) Global Bioenergy Statistics. https://worldenergy.org

[4] Miao, C., Chen, S., Shang, K., Liang, L. and Ouyang, J. (2022) Highly Active Ni–ru Bimetallic Catalyst Integrated with MFI Zeolite-Loaded Cerium Zirconium Oxide for Dry Reforming of Methane. *ACS Applied Materials & Interfaces*, **14**, 47616-47632. https://doi.org/10.1021/acsami.2c12123

[5] Nishimura, A., Sato, R. and Hu, E. (2023) An Energy Production System Powered by Solar Heat with Biogas Dry Reforming Reactor and Solid Oxide Fuel Cell. *Smart Grid*

and Renewable Energy, **14**, 85-106. https://doi.org/10.4236/sgre.2023.145006

[6] Zhang, H., Shuai, Y., Yuan, Y., Guene Lougou, B., Jiang, B., Wang, F., *et al.* (2020) Thermal-Chemical Reaction Characteristics of Ni/Al_2O_3 Catalytic Porous Material Filled Solar Reactor for Dry Reforming of Methane Process. *Applied Thermal Engineering*, **180**, Article ID: 115901. https://doi.org/10.1016/j.applthermaleng.2020.115901

[7] Rathod, V.P., Shete, J. and Bhale, P.V. (2016) Experimental Investigation on Biogas Reforming to Hydrogen Rich Syngas Production Using Solar Energy. *International Journal of Hydrogen Energy*, **41**, 132-138. https://doi.org/10.1016/j.ijhydene.2015.09.158

[8] Zhao, Q., Su, B., Wang, H., He, A., He, R., Kong, H., *et al.* (2021) Mid/Low-Temperature Solar Hydrogen Generation via Dry Reforming of Methane Enhanced in a Membrane Reactor. *Energy Conversion and Management*, **240**, Article ID: 114254. https://doi.org/10.1016/j.enconman.2021.114254

[9] Wang, H., Liu, M., Kong, H. and Hao, Y. (2019) Thermodynamic Analysis on Mid/Low Temperature Solar Methane Steam Reforming with Hydrogen Permeation Membrane Reactors. *Applied Thermal Engineering*, **152**, 925-936. https://doi.org/10.1016/j.applthermaleng.2018.03.030

[10] Zhang, T., Tang, X., Yang, W. and Ma, X. (2023) Comprehensive Performance Study on Reflux Solar Methanol Steam Reforming Reactor for Hydrogen Production. *International Journal of Hydrogen Energy*, **48**, 879-893. https://doi.org/10.1016/j.ijhydene.2022.10.002

[11] Cheng, Z., Leng, Y., Men, J. and He, Y. (2020) Numerical Study on a Novel Parabolic Trough Solar Receiver-Reactor and a New Control Strategy for Continuous and Efficient Hydrogen Production. *Applied Energy*, **261**, Article ID: 114444. https://doi.org/10.1016/j.apenergy.2019.114444

[12] Cheng, Z., Men, J., He, Y., Tao, Y. and Ma, Z. (2019) Comprehensive Study on Novel Parabolic Trough Solar Receiver-Reactors of Gradually-Varied Porosity Catalyst Beds for Hydrogen Production. *Renewable Energy*, **143**, 1766-1781. https://doi.org/10.1016/j.renene.2019.05.137

[13] Ruelas, J., Velázquez, N. and Cerezo, J. (2013) A Mathematical Model to Develop a Scheffler-Type Solar Concentrator Coupled with a Stirling Engine. *Applied Energy*, **101**, 253-260. https://doi.org/10.1016/j.apenergy.2012.05.040

[14] NREL Transforming Energy (2024) NSRDB National Solar Radiation Database. https://nsrdb.nrel.gov/data-viewer

[15] New Energy and Industrial Technology Development Organization (2024) METPV-ASIA. https://www.nedo.go.jp/library/ZZFF_1000038.html

[16] Mohamad, A., Orfi, J. and Alansary, H. (2013) Heat Losses from Parabolic Trough Solar Collectors. *International Journal of Energy Research*, **38**, 20-28. https://doi.org/10.1002/er.3010

[17] Bader, R., Pedretti, A., Barbato, M. and Steinfeld, A. (2015) An Air-Based Corrugated Cavity-Receiver for Solar Parabolic Trough Concentrators. *Applied Energy*, **138**, 337-345. https://doi.org/10.1016/j.apenergy.2014.10.050

[18] García-Valladares, O. and Velázquez, N. (2009) Numerical Simulation of Parabolic Trough Solar Collector: Improvement Using Counter Flow Concentric Circular Heat Exchangers. *International Journal of Heat and Mass Transfer*, **52**, 597-609. https://doi.org/10.1016/j.ijheatmasstransfer.2008.08.004

[19] Nishimura, A., Ohata, S., Okukura, K. and Hu, E. (2020) The Impact of Operating

Conditions on the Performance of a CH_4 Dry Reforming Membrane Reactor for H_2 Production. *Journal of Energy and Power Technology*, **2**, 1-19. https://doi.org/10.21926/jept.2002008

[20] Nishimura, A., Takada, T., Ohata, S. and Kolhe, M.L. (2021) Biogas Dry Reforming for Hydrogen through Membrane Reactor Utilizing Negative Pressure. *Fuels*, **2**, 194-209. https://doi.org/10.3390/fuels2020012

[21] Nishimura, A., Sato, R. and Hu, E. (2024) Performance of an Energy Production System Consisting of Solar Collector, Biogas Dry Reforming Reactor and Solid Oxide Fuel Cell. *Fuels*, **5**, 278-296. https://doi.org/10.3390/fuels5030016

[22] Kreith, F. and Freider, J.K. (1981) Preprints of Thermodynamics and Heat Transfer Applied to Solar Energy. In: Boxwell, M., Ed., *Solar Energy Handbook*, McGraw-Hill, 1.

[23] Dhaundiyal, A. (2022) Rheological Behavior of Air in the Two-Pass Solar Collector. *Frontiers in Energy Research*, **10**, Article 949226. https://doi.org/10.3389/fenrg.2022.949226

[24] Dhaundiyal, A. and Gebremicheal, G.H. (2022) The Stack Effect on the Thermal-Fluid Behaviour of a Solar Collector. *Energies*, **15**, Article 1188. https://doi.org/10.3390/en15031188

[25] Goodfriend, W., Pieters, E.B., Tsvetelina, M., Solomon, A., Ezema, F. and Rau, U. (2024) Development and Improvement of a Transient Temperature Model of PV Modules: Concept of Trailing Data. *Progress in Photovoltaics*: *Research and Applications*, **32**, 399-405. https://doi.org/10.1002/pip.3785

[26] New Energy Foundation (2024) Biogas Power Generation. https://www.nef.or.jp/keyword/ha/articles_ha_02.html

[27] Yanmar (2024) 25kW Class Biogas Power Generation. https://www.yanmar.com/jp/energy/renewable_energy/digestion_gas/

[28] NEDO (New Energy and Industry Technology Development Organization) (2017) Road Map of 2017 of NEDO Fuel Cell and Hydrogen. https://www.nedo.go.jp/content/100871873.pdf

[29] AISIN (2022) General Catalog of ENE-FARM Type S. https://www.aisin.com/jp/product/energy/cogene/enefarm/wp-content/uploads/2024/03/CAT.FC022-4_ENEFARMCATALOG2022.pdf

[30] Enepi (2024) Mean Power Consumption of General Household. https://enepi.jp/articles/265#idx-5

[31] The Japan Society of Mechanical Engineers (1993) JSME Heat Transfer Handbook. Maruzen, 371.